



Elastic Strain Effects on Catalysis of a PdCuSi Metallic Glass Thin Film

Journal:	<i>Physical Chemistry Chemical Physics</i>
Manuscript ID:	CP-ART-10-2014-004924.R1
Article Type:	Paper
Date Submitted by the Author:	22-Nov-2014
Complete List of Authors:	Yang, Yiyi; Brown University, School of Engineering Adit Maark, Tuhina; Brown University, School of Engineering Peterson, Andrew; Brown University, School of Engineering Kumar, Sharvan; Brown University, School of Engineering

Elastic Strain Effects on Catalysis of a PdCuSi Metallic Glass Thin Film

Yiyi Yang, Tuhina Adit Maark, Andrew Peterson and Sharvan Kumar*

School of Engineering, Brown University, Providence, RI 02912, USA

[*Sharvan_Kumar@brown.edu](mailto:Sharvan_Kumar@brown.edu)

The influence of strain on catalytic activity has previously been examined directly by calculations and indirectly by experiments. The origin of the phenomenon has been attributed to strain-induced changes in the catalyst electronic structure. By employing a Pd-based metallic glass film capable of large elastic strains, we provide direct experimental evidence for catalytic activity being differently influenced by mechanically applied uniaxial tensile and compressive strains. We demonstrate the effect on the oxygen reduction reaction with cyclic voltammetry (CV) curves at different strain levels and compare X-ray photoelectron spectrometry (XPS) results for unstrained and strained (in uniaxial tension) specimens to confirm valence electron band shifts. The experimental findings are complemented by electronic structure calculations on single crystal Pd, as well as alloys with Cu and Si. The CV and XPS shifts observed in the experiments are consistent in both direction and magnitude to those predicted by theory for single crystal Pd.

1. Introduction

The ability to apply stress on catalyst surfaces to tune and modulate chemical reactions is implied in “Sabatier’s Principle” and in the “volcano plot”, two widely held concepts in the catalysis field [1]. The peak of a volcano plot corresponds to an optimal

overall reaction rate, determined by two competing elementary reactions with opposite trends under the same driving force. This driving force is typically quantified with the binding energy of a key reaction intermediate, and these binding energies have been shown to be functions of elastic strain. Therefore, a change of the elastic strain level at the catalyst surface is expected to move the operating condition either closer or further away from the optimal condition, thereby increasing or decreasing the total reaction rate.

The idea of using strain to modify catalytic reaction rates has been evolving rapidly over the past two decades. Theoretically, simulations indicate that strain can influence the catalytic behavior by changing the bond strength between adsorbed atoms or molecules and the catalyst surface [2-4]. These calculations show that the misfit lattice strain can change the width of the d-band, and then further modify the reactivity of the strained surface by shifting the d-band center relative to the Fermi energy of the catalyst surfaces [5-10].

Most experiments probing the elastic strain effect on catalytic activity have been confined to the use of misfit strains, which is usually induced by epitaxial deposition. Work on monolayers of Pd epitaxially deposited on various fcc and hcp metals [9] validated the lattice strain induced d-band shift during H desorption. Other studies have used Pt monolayer catalysts on nanoparticles of other metals and metal oxides [4,11,12] and single crystal plane surfaces [13-15]. An interesting recent approach has used a dealloying method to achieve strain [16]. The increased catalytic activity of dealloyed bimetallic core/shell nanoparticles [16-18] and dealloyed thin films [19,20] have been attributed to the d-band center shift due to mismatch strains between the outer noble-metal-rich surface and the inner cores or substrates.

There are, however, limitations in these theoretical and experimental studies. Generally, the elastic strain on the surface in these studies is only controlled under ideal conditions, such as monolayers on single-crystal substrates, or in other cases, simply estimated without consideration being given to relaxation by misfit dislocations at interfaces. In addition, it is known that the altered catalytic activity of the dealloyed nanoparticles and thin films are due to a combined effect of (1) altered catalyst surface area [21], (2) the shift of the d-band center due to the induced strain [6,7], and (3) chemical “ligand” effects resulting from the substrate [8,10]. Additionally, the misfit and dealloying approach require separate samples to be prepared for each strain level. As a result, the strain effect in these systems is not conclusively isolated and quantified.

The simplest means to unambiguously demonstrate a strain effect in catalysis would be to externally apply mechanical strain to a single catalyst sample. However, it is generally believed that such large elastic strain levels cannot be achieved by common metal catalysts. Therefore, to demonstrate a direct strain effect as a means to control catalytic activity using externally applied elastic strain, and to quantitatively and systematically measure this effect, it is necessary to find novel metallic materials capable of high yield strengths and low elastic moduli that together can result in “large” elastic strains. There are two categories of modern materials that satisfy the strength criterion: metal nanopillars [22] and metallic glasses [23]. Additionally, Pd- and Cu-based metallic glasses display moduli that are lower than those for pure Pd and Cu, respectively [24], and (unstrained) Pd-based glasses have been shown to exhibit catalytic activity in electrochemical applications [25].

In this study, a $\text{Pd}_{77}\text{Cu}_{16}\text{Si}_7$ metallic glass thin film deposited on a polymethyl

methacrylate (PMMA) substrate is used as a model material to systematically characterize and measure the elastic strain effect on electrochemical behavior during the oxygen reduction reaction (ORR), in a uniaxial testing configuration. We provide experimental results, supported by theoretical predictions developed using density functional theory (DFT), that demonstrate that compressive elastic strain can enhance the catalytic activity while tensile elastic strain suppresses it during ORR. Through X-ray photoelectron spectroscopy (XPS) of unstrained and strained specimens, we confirm that uniaxial tensile strain shifts the valence band structure (VBS) of the thin film catalyst, the direction of the shift and its magnitude being consistent with those predicted by electronic-structure calculations.

2. Experimental methods

The Pd-Cu-Si master alloy was prepared by melting a mixture of commercially available high purity palladium, copper, and silicon shots in zirconia crucibles, within a high purity argon environment, by heating the mixture to $> 1600^{\circ}\text{C}$. The molten alloy was then bottom-poured from the crucible into a split Cu mold. Multiple polymethyl methacrylate (PMMA) tensile and compression specimen templates were machined, and a 20-nm thick $\text{Pd}_{77}\text{Cu}_{16}\text{Si}_7$ film was deposited by e-beam evaporation on one face of each of these specimens using the Pd-Cu-Si master alloy as a source (details shown in Figure 1c-f). Good adhesion between a Pd-based metallic glass thin film and commercially available PMMA substrate has been recently demonstrated [26], and this ensures the effective transfer of stress/strain from the PMMA substrate to the glass film. Such e-beam deposited specimens were characterized by scanning electron microscopy and X-ray

diffraction. The elemental composition of the metallic glass film was measured using energy dispersive spectrometry by point scans at six randomly chosen spots on each film and compared to the nominal composition.

The electrochemical measurements were conducted in a homemade three-electrode cell, which was installed onto an Instron 4505 tensile/compression frame. This setup allowed *in-situ* measurements of electrochemical responses while the specimen was under different loading conditions, *i.e.*, uniaxial tension and compression, as shown in Figure 1a,b. Potentials were determined using a Ag/AgCl reference electrode (Pine Research Instrumentation). The cyclic voltammetry (CV) tests were performed in high purity, oxygen-purged-0.1 M perchloric acid solution at room temperature. Pure Pt wire was used as the counter electrode. The working electrodes were the Pd₇₇Cu₁₆Si₇ thin films deposited on PMMA substrate. An Autolab potentiostat (Metrohm USA Inc.) was used for the electrochemical measurements of catalytic activity of the films for ORR. The CV scan rate of all the measurements was 20 mV/sec.

To obtain the valence band structure (VBS) of the Pd metallic glass film on the PMMA substrate in the unstrained and strained conditions, a tensile deformation stage utilizing flat, sub-scale “bow-tie” configuration PMMA tensile specimens was designed for the X-ray photoelectron spectroscopy (XPS) measurements of specimens subjected to elastic strains. A 20-nm thick Pd₇₇Cu₁₆Si₇ film was deposited on one face of these PMMA specimens. Valence band structure measurements were performed by XPS using monochromatic Al K α radiation on a 5500 Multi-technique Surface Analyzer (Physical Electronics, Inc.). All the surfaces were sputter-cleaned for six seconds before XPS measurements were performed. The step size for all the XPS scans was 50 meV. The

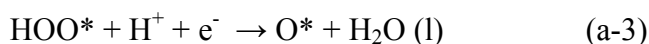
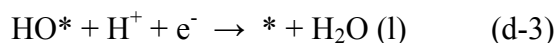
specimen was mounted in this stage and first scanned in the XPS prior to any deformation. It was then taken out and loaded ex-situ in the stage to ~1.5% elastic strain (The strain was calculated based on displacement measurements using a pair of Vernier calipers), then re-inserted into the chamber and evaluated again. Lastly, the stage was taken out once more, the specimen was unloaded completely and then the specimen and stage were re-inserted into the XPS chamber and similarly characterized.

3. Computational methods

Electronic structure calculations were performed using the open-source planewave, density-functional theory (DFT) code “DACAPO” within the Atomic Simulation Environment (ASE). [27,28] The DFT calculations employed Vanderbilt ultrasoft pseudopotentials [29] and the revised Perdew–Burke–Ernzerhof RPBE exchange-correlation functional [30]. The effect of uniaxial strain on ORR activity was studied on the Pd(111) surface, modeled as a (2×2) unit cell with four layers (of which the bottom two layers were constrained) and 20 Å vacuum. The slab model of the Pd(111) surface is shown in Figure 2a. In the strained surfaces, the induced relaxations in response to the applied in-plane uniaxial strain along $[-110]$ or $[11-2]$ directions were explicitly taken into account. A planewave cut-off of 450 eV, density cut-off of 500 eV, and $4 \times 4 \times 1$ k -point mesh were used for all geometry optimizations.

The literature focuses on two major mechanisms for the oxygen reduction reaction (ORR): the dissociative (in which the O-O bond breaks upon adsorption) and the associative (in which the O-O bond is intact upon adsorption as OOH, and electrochemically broken to produce adsorbed O). Both mechanistic possibilities will be

considered in this work. The dissociative and associative mechanisms are outlined in eqs. (d-1) to (d-3) and (a-1) to (a-5) respectively.



In the above equations, the * represents an adsorption site on the surface. It is noted that the last two steps in both the mechanisms are the same. All the intermediates were adsorbed at their most favored sites over unstrained Pd(111).

The free energies were obtained by adding zero-point energy and entropic corrections from Ref. [31] and solvation corrections from Ref. [32]. The electrochemical steps were captured thermodynamically by employing the computational hydrogen electrode model [31] in which the reaction free energy of a step which is associated with a proton/electron ($\text{H}^+ + \text{e}^-$) transfer, such as $\text{A}^* + (\text{H}^+ + \text{e}^-) \rightarrow \text{AH}^*$, is thermodynamically equivalent to hydrogen gas at 0 V vs RHE; *i.e.*, $\text{A}^* + \frac{1}{2} \text{H}_2 \rightarrow \text{AH}^*$. The reaction potential is adjusted from 0 V with the relationship of $\Delta G_U = -e U$. In accordance with the literature, the experimental reaction free energy (2.46 eV) for $\text{H}_2\text{O} \rightarrow \frac{1}{2} \text{O}_2 + \text{H}_2$ was used to calculate the free energy of O_2 , coupled with H_2O and H_2 as references. This ensures a consistent set of molecular free energies.

Complete descriptions of metallic glasses are typically not accessible within periodic density functional theory calculations. However, to approximate the effect of the presence of Cu and Si in the bulk metallic glass system ($\text{Pd}_{77}\text{Cu}_{16}\text{Si}_7$) calculations were performed on periodic Pd, $\text{Pd}_{0.75}\text{Cu}_{0.25}$, and $\text{Pd}_{0.75}\text{Si}_{0.25}$. The Pd was modeled as a fcc unit cells while the binary Pd-Cu compositions were modelled using the $L1_2$ lattice so that the periodic Pd unit cell is comprised of four Pd atoms and in $\text{Pd}_{0.75}\text{Cu}_{0.25}$, and $\text{Pd}_{0.75}\text{Si}_{0.25}$ atomic ratio of Pd:Cu/Si is 3:1 with Pd occupying the face-centered sites. The lattice constants of Pd, $\text{Pd}_{0.75}\text{Cu}_{0.25}$, and $\text{Pd}_{0.75}\text{Si}_{0.25}$ were calculated (by relaxing the unit cells until the stress became zero) to be 4.016, 3.949, and 3.919 Å respectively. As derivation of elastic stiffness constants (s_{11} , s_{12} , and s_{44}) involves applying different distortions to the unit cell, higher cut-offs (650 eV for plane waves and 800 eV for density) were used along with $8 \times 8 \times 8$ k -points for each of the three systems considered in this work. These were then utilized to evaluate the induced relaxations in the orthogonal directions as a result of application of a uniaxial strain along the [001], [110], and [111] directions using Poisson's ratio. In order to apply the strains along [110] and [111] directions new unit cells were created. The structures of all the unit cells that have been used are presented in Figures 2b-i. All geometry and electronic relaxations for systems with applied strain along [001] direction were carried out at 340 eV planewave cut-off, 500 eV density cut-off, and $8 \times 8 \times 8$ k -points. For the larger unit cells employed when applied strain was along [110] or [111] direction, the k -point mesh was changed to the sparser $4 \times 4 \times 4$. For all projected density of states (PDOS) calculations, $6 \times 6 \times 6$ k -points were used with a cut-off radius of 1.0 Å. The d-band center was derived as the central moment of the d-band: $\epsilon_d = \int \rho E dE / \int \rho dE$.

4. Results and discussion

4.1 Pd₇₇Cu₁₆Si₇ thin film characterization

The as-deposited film was found to be continuous and smooth and devoid of microcracks or microvoids when examined in a scanning electron microscope (SEM) (Figure 3a). X-ray diffraction (XRD) using monochromatic Cu-K α radiation confirmed the metallic glass nature of the specimens evidenced by the single broad peak at $2\theta \approx 42^\circ$ in the diffraction pattern (Figure 3b). The elemental composition of the metallic glass film was measured using energy dispersive spectrometry (EDS) by point scans at six randomly chosen spots on each film and compared to the nominal composition. The composition of the deposited thin film varied within one atomic percent for the different specimens.

No microcracks or “shear bands” (a plastic deformation mode for metallic glasses) were present in the films deformed to 1.5% strain (Figure 3c), which confirmed that all the specimens were deformed within the elastic regime. In contrast, when a specimen was deformed to 2.5% strain, and subsequently examined in the SEM (Figure 3d), shear bands at an inclination to the tensile axis were observed, characteristic of metallic glasses [33,34], clearly illustrating that the elastic limit for this metallic glass film lies between 1.5% and 2.5% strain.

4.2 Strain effects on electrochemical behavior

4.2.1 Experiments

To understand the effects of an externally applied macroscopic elastic strain on

the catalytic response of the Pd₇₇Cu₁₆Si₇ metallic glass film during ORR, tension and compression specimens were deformed within an electrochemical cell attached to an Instron-type uniaxial tension/compression load-frame.

During deformation, the CV response of Pd₇₇Cu₁₆Si₇ films was collected in steps at 0%, 0.5%, 1.0%, and 1.5% engineering strains (determined by crosshead displacement) during the first loading cycle. To verify that the specimen only experienced elastic deformation, the CV test was repeated after unloading the sample (*i.e.*, 0% strain after the 1.5% strain excursion); furthermore, the specimen was loaded directly for a second time to 1.5% strain and a CV scan was performed again and compared to the first excursion to this strain level to verify reproducibility. Lastly, at each of these strain levels (*i.e.*, 0% → 0.5% → 1.0% → 1.5% → 0% → 1.5%), five slow potential scan cycles were performed at 20 mV/s between -0.1 V and 0.7 V *vs.* the Ag/AgCl reference electrode at room temperature. Thus, overall, the tensile specimen was subjected to 30 cycles.

The CV response of the Pd₇₇Cu₁₆Si₇ metallic glass film at four different tensile strain levels during the first loading cycle is shown in Figure 4a. (Note: The third cathodic sweep for each CV scan is shown in Figure 4a-f). CV curves collected at different strain levels revealed a continuous negative shift with an increase in magnitude of the tensile strain indicating that tensile strain can suppress the catalytic activity of the metallic glass films during ORR. The CV curves at 0% strain prior to the first loading cycle, and after the first loading cycle are compared in Figure 4b, while the CV curves at 1.5% strain for the first and second loading cycles are compared in Figure 4c. The observed overlap in Figure 4b confirms the fully reversible (elastic) nature while Figure 4c confirms reproducibility. Thus the observed systematic shifts in Figure 4a are thought

to be a direct consequence of mechanically imposed elastic tensile strain.

Similar experiments were performed in uniaxial compression and the response of the Pd₇₇Cu₁₆Si₇ film at four different compressive strain levels during the first loading cycle are shown in Figure 4d. In contrast to Figure 4a, the CV curves revealed a continuous positive shift with an increase in magnitude of the compressive elastic strain, implying that compressive strain enhances the catalytic activity of the metallic glass films during ORR. The data in Figures 4e and 4f correspond to those in Figures 4b and 4c respectively (except, in compression) and confirm reversibility and reproducibility. As in the case of the tensile specimen, the compression specimen experiences a total of 30 cycles.

To ensure that the as-deposited film is stable over the total number of cycles it experiences in the above tests, CV scans were performed on an as-deposited film between -0.1V and 0.7V during ORR when the film was in the strain-free state for a total of 100 cycles. The CV scan for the first cycle, the 50th cycle and the 100th cycle are presented in Figure 5 and it is evident that they superimpose on each other. This confirms that the observed shifts in Figures 4a, d are a consequence of the mechanically applied strain and the film is stable at least for the first 100 cycles.

4.2.2 Simulations

Since two major mechanisms are discussed in the literature for the reduction of O₂ to H₂O, we present results of the expected activity response to strain for each proposed mechanism. We will show that both mechanisms show a similar predicted direction and magnitude of the response, which are consistent with the presented experimental

findings.

Dissociative mechanism: From equations (d-1) to (d-3) it is evident that there are two intermediates of concern: O* and HO*. On Pd(111) both of these are preferentially adsorbed over an fcc site as shown in Figure 6. When considering the dissociative mechanism for ORR, it was found that the direction of the applied in-plane uniaxial strain, *i.e.* [-110] versus [11-2], had minimal effect on the binding energies of the intermediates and thereby on the free energy changes and ORR activity. So, in this section, only the results for strain along the [11-2] direction are presented. Figure 6 shows the free energy diagrams for ORR on -2.5%, 0.0%, and +2.5% uniaxially strained Pd(111) surfaces at $U = 1.23$ V. Compared to the unstrained surface, tensile strain strengthens while compressive strain weakens the adsorption of O and OH on Pd(111). Formation of O* is downhill in energy but the protonation steps for O* to HO* and HO* to H₂O are uphill in free energy. It is observed from Figure 7a that at all strains $\pm 2.5\%$ tested, the protonation of HO* to H₂O *i.e.* step (d-3) has the largest uphill ΔG . The corresponding values can be used to calculate activity (A) as the limiting potential (U_L):

$$A = U_L = 1.23 - \Delta G(d-5)/e \quad (1)$$

Expansion increases the “uphillness” of step (d-3) while compression decreases it; as a consequence the ORR activity of Pd(111) in Figure 7b is enhanced on compression and reduced with tensile strain compared to the unstrained Pd(111).

Associative mechanism: Steps (a-1) to (a-5) illustrate that the intermediates of interest are: O₂*, HOO*, O*, and HO*. O₂ is adsorbed in a top-fcc-bridge orientation and OOH has a top-bridge-top adsorption over the Pd(111) surfaces. These geometries are displayed in Figure 8. The free energy diagram corresponding to associative mechanism

over Pd(111) uniaxially strained along [11-2] direction at $U = 1.23$ V is also shown in Figure 8. Formation of O_2^* and O^* is downhill in energy and all other protonation steps are uphill in energy amongst which O_2^* protonation to HOO^* has the largest free energy change. The free energy of this elementary step, $\Delta G(a-2)$, decreases with compression and increases on expansion (see Figure 9a). As the free energy of the potential-limiting step becomes smaller, the ORR activity (quantified by the limiting potential) is predicted to increase; *i.e.*, it is enhanced on compression, as shown in Fig. 9b.

4.2.3 Comparing experiments and simulations

The voltage shift resulting from mechanical strain at a current density of 0.2 mA/cm² was extracted from the experimental data in Figures 4a and 4d for tension and compression loading respectively, and is plotted as a function of strain in Figure 10a. (No point is shown for the unstrained specimen as the rest of the data are with reference to the unstrained condition.) Each datum point is an average of four specimens tested to a particular strain level and the error bar on each point denotes the spread in data for the four specimens. The response is almost linear with strain. An average total shift of about -30 mV occurs at the current density of 0.2 mA/cm² at 1.5% tensile strain compared to that for the unstrained condition (0% strain); the corresponding change for a compressive strain of -1.5% is about $+50$ mV.

In theoretical studies [35-37], the limiting potential U_L obtained from DFT calculations has been demonstrated to provide an indication of trends in experimental onset potentials. Figure 10b shows the voltage shift estimated as the shift in limiting potential (ΔU_L) for Pd (111) surfaces under dissociative and associative mechanisms for

ORR as a result of uniaxial strain. In general, U_L shifts up (enhanced catalytic activity) for compression and down (depressed catalytic activity) for extension by tens of millivolts over the range of -1.5 to +1.5% strain and is qualitatively consistent with experiments. If ORR proceeds via the associative mechanism over the Pd (111) surface, ΔU_L is affected by the direction of in-plane uniaxial strain. When the applied strain is along the [-110] direction, the ORR limiting potential does not decrease as much on expansion, but increases up to 12 mV with a strain of -1.5% similar to when strain is along [11-2] direction. The latter however, causes a stronger ΔU_L of -10 mV under a tensile strain of +1.5%. Overall, the voltage shift from experiments (in Figure 10a for the metallic glass) and ΔU_L from theoretical calculations (Figure 10b for single crystal Pd) show reasonable agreement in trend and magnitude, regardless of the assumed mechanism.

4.3 Strain effects on valence band structure

4.3.1 Experiments

XPS was used to obtain the VBS of the Pd₇₇Cu₁₆Si₇ metallic glass film on the PMMA substrate in the unstrained and strained conditions. The specimen was characterized in the XPS using a tensile straining stage, first, prior to any deformation, then after loading to ~1.5% elastic strain, and then again after fully unloading the specimen. The experimental results in the form of the VBS are presented in Figures 11a,b. In Figure 11a, the two overlapping spectra correspond to the specimen prior to loading (initial condition – 0% strain) and after complete unloading (final condition – 0% strain) verifying reversibility and reproducibility. In Figure 11b, we compare the initial

condition (0% strain) with the tensile strained condition (1.5% elastic strain) and demonstrate a visible upshift in the valence band, the magnitude being of the order of 50-100 meV. It is worth noting that the measured VBS of the thin film is a combined effect of the Pd 4d and Cu 3d bands.

4.3.2 Simulations

Although calculations of the shift in the Pd d-band in an amorphous state are not practical with modern electronic structure methods, we can use calculations on related crystalline systems in order to estimate the magnitude of the changes. Specifically, we examined systems of pure Pd and of Pd doped with either Si or Cu, to capture the variety of neighboring atoms experienced by Pd in glasses. The projected density of states (PDOS) was calculated from DFT for periodic Pd, Pd_{0.75}Cu_{0.25}, and Pd_{0.75}Si_{0.25} systems under a uniaxial strain along the [001], [110], and [111] directions. When the strain was applied along (a) [001], these structures were modeled as fcc unit cells (for Pd) or with the L1₂ lattice (Pd_{0.75}Cu_{0.25}, and Pd_{0.75}Si_{0.25}), (b) [110], a unit cell with [001], [-110], and [110] as *x*, *y*, and *z* axes, respectively was used, and (c) [111], a unit cell with [-110], [11-2], and [111] as *x*, *y*, and *z* axes, respectively was employed. In each case the induced relaxations along the orthogonal directions were included in the model (Figures 2b-i). For comparison with experiments, uniaxial strains of -1.5 and +1.5% were applied along [001], [110], and [111] directions by suitably varying the lattice parameters of the three systems. As an example, the PDOS plots of the most perturbed Pd atom in each unit cell when the applied strain is along [111] direction are shown in Figure 11c-e for the structure corresponding to Figure 1h.. It is seen that as the strain is increased from -1.5%

to +1.5% the d-band shifts up, consistent with the XPS results. The magnitude of shift is similar to that observed experimentally in Figure 11b.

Table I summarizes the predicted shifts in d-band center ($\Delta\varepsilon_d$) for each system on application of a +1.5% tensile strain along different directions. It can be inferred from Table I that the direction of applied uniaxial strain and electronic effects due to presence of Cu or Si in $\text{Pd}_{0.75}\text{Cu}_{0.25}$ and $\text{Pd}_{0.75}\text{Si}_{0.25}$ only marginally affect the calculated shift (relative to the unstrained counterparts) in the d-band center, $\Delta\varepsilon_d$. In general the calculated d-band shift for Pd atoms in various crystalline pure, Cu-doped, and Si-doped environments is of the same direction and magnitude as the experimentally observed shift in the VBS from XPS measurements on the +1.5%-strained metallic glass thin film.

5. Conclusions

In summary, we provide direct experimental evidence supported by theoretical calculations for catalytic activity being differently influenced by mechanically applied uniaxial tensile and compressive strains. We do this using the oxygen reduction reaction as an example. Further, by comparing XPS results for unstrained and strained (in uniaxial tension) specimens, we confirm valence electron band shifts that are consistent in both direction and magnitude to those predicted by theory for single crystal Pd. These results suggest the possibility of improving and controlling electrochemical reaction rates using cyclic loading with potential implications in areas such as energy conversion, energy storage, and sensors, and on a more fundamental level, provide key insights into surface reactivity.

This material is based upon work supported by the U.S. Army Research Laboratory and the U.S. Army Research Office under the Multi University Research Initiative MURI grant number W911NF-11-1-0353 at Brown University.

References

- [1] J.K. Nørskov, T. Bligaard, J. Rossmeisl, and C.H. Christensen, *Nat. Chem.* **1**, 37 (2009).
- [2] M. Mavrikakis, B. Hammer, and J.K. Nørskov, *Phys. Rev. Lett.* **81**, 2819 (1998).
- [3] W. Tang and G. Henkelman, *J. Chem. Phys.* **130**, 194504 (2009).
- [4] X.J. Wang, H. Inada, L. Wu, Y. Zhu, Y. Choi, P. Liu, W. Zhou, and R. Adzic, *J. Am. Chem. Soc.* **131**, 17298 (2009).
- [5] A.J. Appleby, *Catal. Rev.* **4**, 221 (1970).
- [6] B. Hammer and J.K. Nørskov, *Adv. Catal.* **45**, 71-129 (2000).
- [7] J. Greeley, and M. Mavrikakis, *Annu. Rev. Phys. Chem.* **53**, 319 (2002).
- [8] J.R. Kitchin, J.K. Nørskov, M.A., Barteau, and J.G. Chen, *Phys. Rev. Lett.* **93**, 156801 (2004).
- [9] L.A. Kibler, A.M., El-Aziz, R. Rüdiger Hoyer, and D.M. Kolb, *Angew. Chemie Intl. Ed.* **44**, 2080 (2005).
- [10] T. Adit Maark and A.A. Peterson, *J. Phys. Chem. C* **118**, 4275 (2014).
- [11] K. Sasaki, L. Zhang, and R.R. Adzic, *Phys. Chem. Chem. Phys.* **10**, 159 (2008).
- [12] K. Sasaki, and R.R. Adzic, *J. Electrochem. Soc.* **155**, B180 (2008).
- [13] W.P. Zhou, X. Yang, M.B. Vukmirovic, B.E. Koel, J. Jiao, G. Peng, M. Mavrikakis, and R.R. Adzic, *J. Am. Chem. Soc.* **131**, 12755 (2009).
- [14] V.R. Stamenkovic, N.M. Markovic, and P.N. Ross, *J. Electroanal. Chem.* **500**, 44 (2001).
- [15] V.R. Stamenkovic, B. Fowler, B.S. Mun, G. Wang, and P.N. Ross, *Science* **315**, 493 (2007).
- [16] P. Strasser, S. Koh, T. Anniyev, J. Greeley, K. More, C. Yu, Z. Liu, S. Kaya, D. Nordlund, H. Ogasawara, M.F. Toney, and A. Nilsson, *Nat. Chem.* **2**, 454 (2010).
- [17] P. Mani, R. Srivastava, and P. Strasser, *J. Phys. Chem. C* **112**, 2770 (2008).
- [18] L. Gan, M. Heggen, S. Rudi, and P. Strasser, *Nano Lett.* **12**, 5423 (2012).
- [19] R. Yang, J. Leisch, P. Strasser, and M.F. Toney, *Chem. Mater.* **22**, 4712 (2010).
- [20] H. Liu, P. He, Z. Li, and J. Li, *Nanotechnology* **17**, 2167 (2006).
- [21] M.T. Paffet, G.J. Beery, and S. Gottesfeld, *J. Electrochem. Soc.* **135**, 1431 (1988).
- [22] H. Bei, S. Shim, E.P. George, M.K. Miller, E.G. Herbert, and G.M. Pharr, *Scripta Mater.* **57**, 397 (2007).
- [23] W.L. Johnson, *MRS Bull.* **24**, 42 (1999).
- [24] W. Wang, *Nature Mater.* **11**, 275 (2012).
- [25] M. Carmo, R.C. Sekol, S. Ding, G. Kumar, J. Schroers, and A.D. Taylor, *ACS Nano*

- 5, 2979 (2011).
- [26] E. Soinial, P. Sharma, M. Heino, K. Pischow, A. Inoue, and H. Hanninen, *J. Phys.: Conference Series* **144**, 012051 (2009).
- [27] Dacapo and ASE are open-source codes available from the Department of Physics at the Technical University of Denmark, at <https://wiki.fysik.dtu.dk>.
- [28] S.R. Bahn and K.W. Jacobsen, *Comput. Sci. Engg.* **4**, 56 (2002).
- [29] D. Vanderbilt, *Phys. Rev. B* **41**, 7892 (1990).
- [30] B. Hammer, L.B. Hansen, and J.K. Nørskov, *Phys. Rev. B* **59**, 7413 (1999).
- [31] J.K. Nørskov, J. Rossmeisl, A. Logadottir, L. Lindqvist, J.R. Kitchin, T. Bligaard, and H. Jónsson, *J. Phys. Chem. B* **108**, 17886 (2004).
- [32] G.S. Karlberg, J. Rossmeisl, and J.K. Nørskov, *Phys. Chem. Chem. Phys.* **9**, 5158 (2007).
- [33] A.C. Lund and C.A. Schuh, *Intermetallics* **12**, 1159 (2004).
- [34] M. Zhao, and M. Li, *Appl. Phys. Lett.* **93**, 241906 (2008).
- [35] G.S. Karlberg, J. Rossmeisl, and J.K. Nørskov, *Phys. Chem. Chem. Phys.* **9**, 5158 (2007).
- [36] V. Viswanathan, H.A. Hansen, J. Rossmeisl, and J.K. Nørskov, *J. Phys. Chem. Lett.* **3**, 2948 (2012)
- [37] C. Shi, H.A. Hansen, A.C. Lausche, and J.K. Nørskov, *Phys. Chem. Chem. Phys.* **16**, 4720 (2014)

Figure Captions:

Figure 1. Illustrations of *in-situ* (a) uniaxial tension and (b) uniaxial compression CV test set-up; (c-e) schematics of the dog-bone geometry tension specimen (c) and rectangular block compression specimen (d) of PMMA with a Pd₇₇Cu₁₆Si₇ metallic glass thin film deposited on the gauge section are shown. In (e), a side profile of the tension specimen is shown with the electrical connection to the glass film, and in (f) a photograph of a uniaxial tension specimen is presented.

Figure 2. (a) Slab model used for constructing pure Pd(111) surfaces is depicted from both side and top views and bulk unit cell used when uniaxial strain is applied along (b) [001] direction in pure Pd, (c) [110] direction in pure Pd, (d) [111] direction in pure Pd, (e) [001] direction in Cu or Si doped Pd, (f) [110] direction in Cu or Si doped Pd whose 2 × 2 × 2 supercell is (g), and (h) [111] direction in Cu or Si doped Pd whose 2 × 2 × 2 supercell is (i).

Figure 3. (a) Secondary electron SEM image shows a uniformly deposited 20 nm-thick Pd-Cu-Si film on a PMMA substrate. (b) XRD pattern confirms the as-deposited thin film to be a glass. Post-deformed thin film shows (c) no evidence for plastic deformation after 1.5% strain whereas (d) shear bands confirm irreversible deformation after 2.5% strain.

Figure 4. Cyclic voltamograms of Pd₇₇Cu₁₆Si₇ metallic glass thin film deposited on a PMMA substrate: (a-c) *in-situ* tension tests and (d-f) *in-situ* compression

tests; (a,d) at different strain levels using a scan rate of 20mV/s. Cathodic sweeps are shown. Comparison of cyclic voltamograms of the metallic glass thin film at (b,e) 0% strain before and after unloading from 1.5% strain, and (c,f) at 1.5% strain in the 1st and 2nd tensile loading cycles. (b,c,e,f) show the reproducible and reversible nature of the scans. Note that the third cycle from each test is shown.

Figure 5. Cyclic voltamograms (cathodic sweeps) for the first, the 50th, and the 100th cycles for a Pd₇₇Cu₁₆Si₇ metallic glass thin film deposited on a PMMA substrate, confirming adequate stability of the as-deposited film for the duration of the straining tests depicted in Figure 4.

Figure 6. Optimized geometries of O and OH adsorbed Pd(111) and free energy diagram at $U = 1.23$ V for ORR via dissociative mechanism on Pd(111) surfaces uniaxially strained along [11-2] direction.

Figure 7. Variation of (a) reaction free energies of protonation of O* and HO* steps and (b) ORR activity (via dissociative mechanism) in terms of the limiting potential (U_L) of Pd(111) surfaces at $U = 1.23$ V with applied uniaxial strain along [11-2] direction.

Figure 8. Optimized geometries of O₂ and HOO adsorbed Pd(111) and free energy diagram at $U = 1.23$ V for ORR via associative mechanism on Pd(111) surfaces uniaxially strained along [11-2] direction.

Figure 9. Variation of (a) reaction free energies of protonation of HOO* step and (b) ORR activity (via associative mechanism) in terms of the limiting

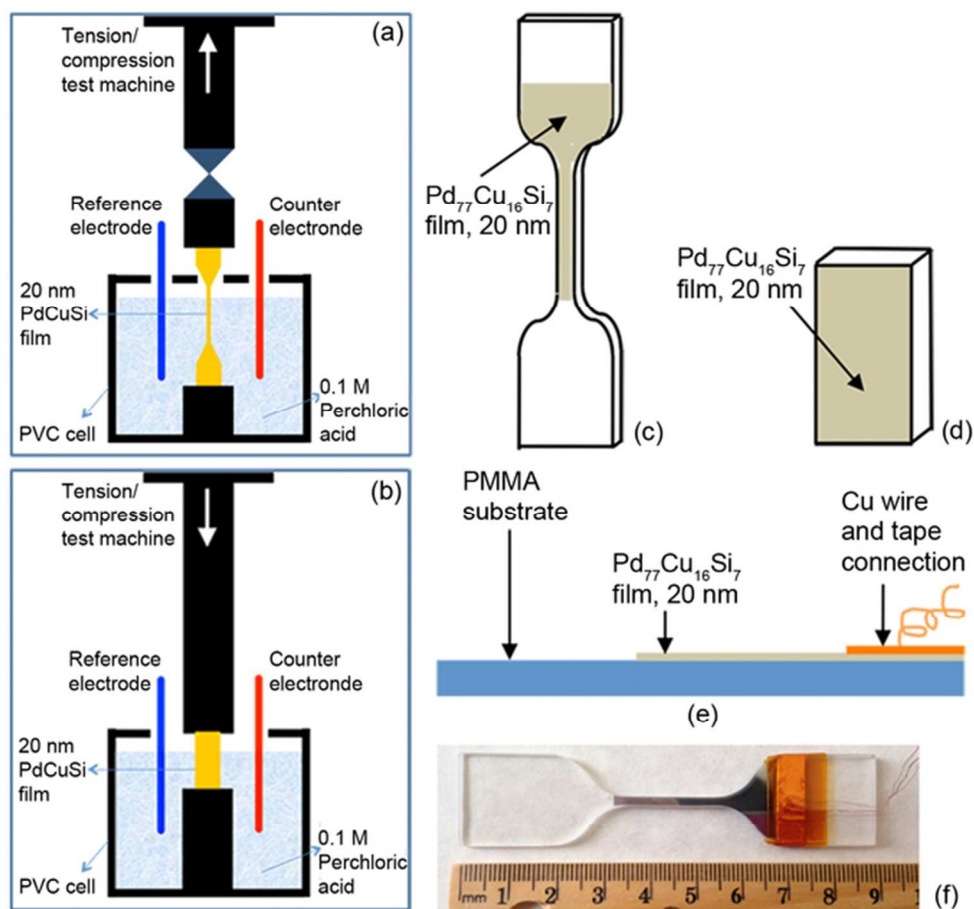
potential (U_L) of Pd(111) surfaces at $U = 1.23$ V with applied uniaxial strain along [11-2] direction.

Figure 10. (a) CV curve shifts relative to the zero strain level for different tensile and compressive strains at a current density of 0.2 mA/cm^2 . The error bars bracket the entire range of five measurements. (b) Shift in limiting potential from calculations for ORR on Pd (111) surface, as a function of uniaxial strain based on associative and dissociative mechanisms.

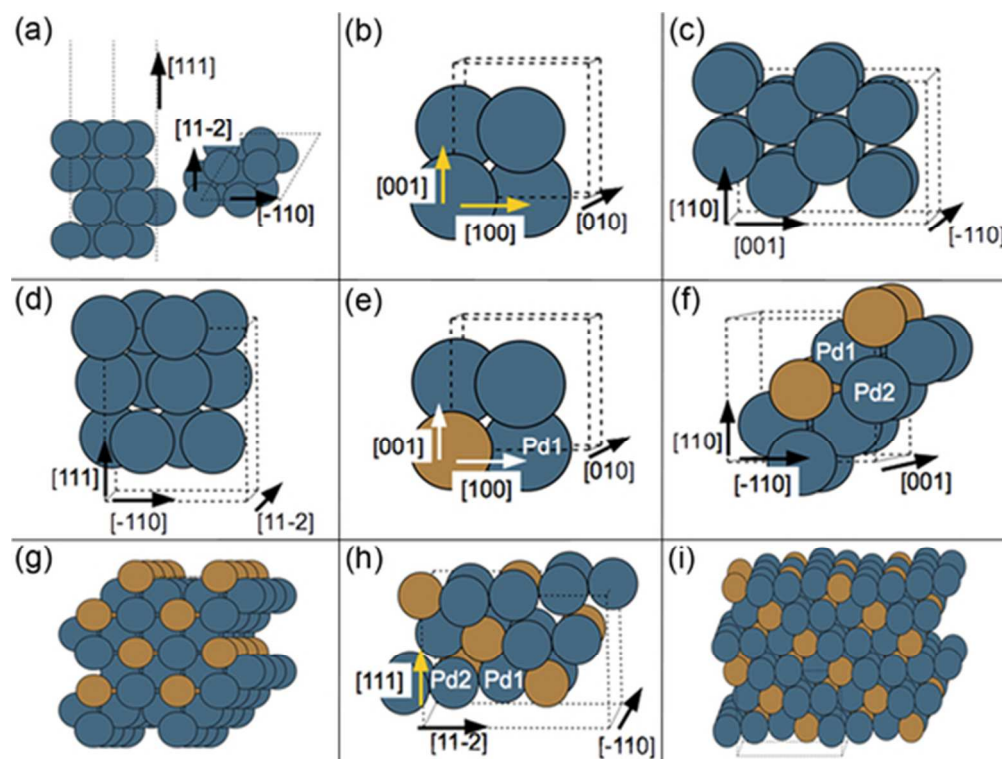
Figure 11. (a) Valence Band Structure (VBS) from XPS experiments of $\text{Pd}_{77}\text{Cu}_{16}\text{Si}_7$ metallic glass thin film at 0% strain (before loading and after unloading from 1.5% tensile strain). (b) An up-shift of the VBS of the same thin film specimen at 1.5% strain (red curves) relative to the VBS obtained before deformation (black dashed curve). Computed projected density of states (PDOS) plots for Pd d-states in periodic (single crystal) (c) Pd, (d) $\text{Pd}_{0.75}\text{Cu}_{0.25}$, and (e) $\text{Pd}_{0.75}\text{Si}_{0.25}$ -1.5 and +1.5% uniaxially strained along [111] direction.

Table I: Shift in d-band center ($\Delta\varepsilon_d$) of periodic Pd, Pd_{0.75}Cu_{0.25}, and Pd_{0.75}Si_{0.25} on application of +1.5% uniaxial strain along [001], [110], and [111] directions relative to the unstrained counterparts.

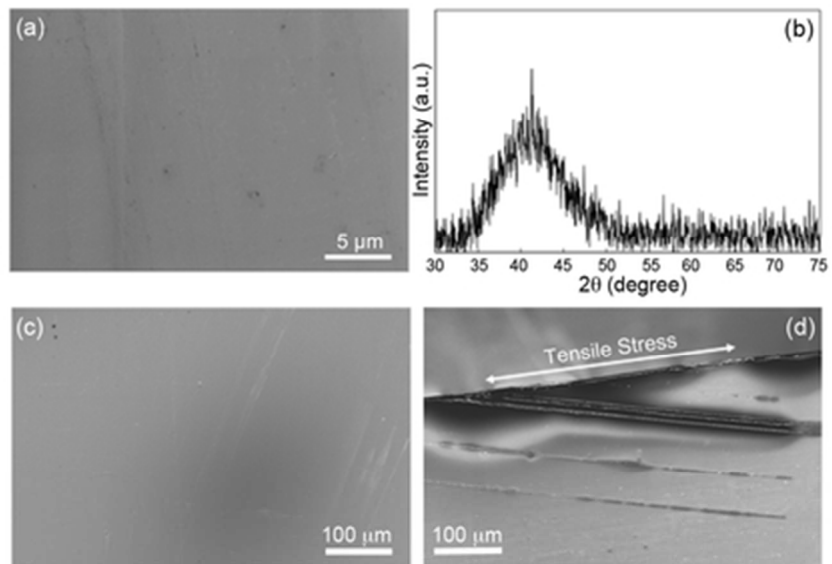
System	$\Delta\varepsilon_d$ at +1.5% strain (meV)		
	[001]	[110]	[111]
Pd	+6	+10	+11
Pd_{0.75}Cu_{0.25}	+24	+18	+13
Pd_{0.75}Si_{0.25}	+17	+37	+18



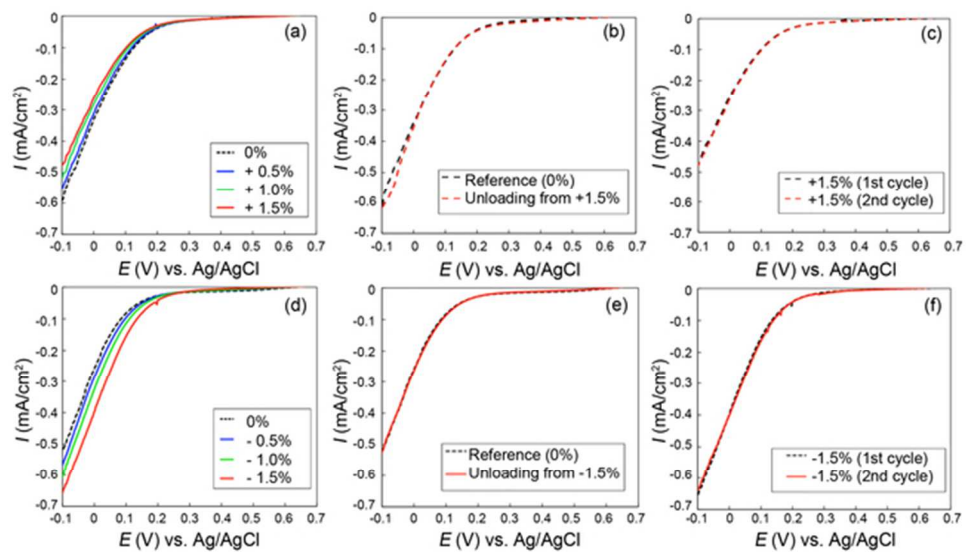
58x54mm (300 x 300 DPI)



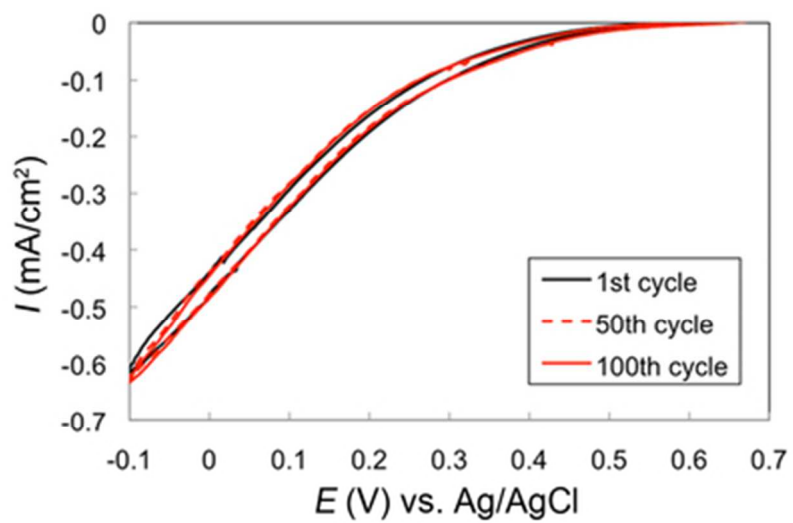
47x35mm (300 x 300 DPI)



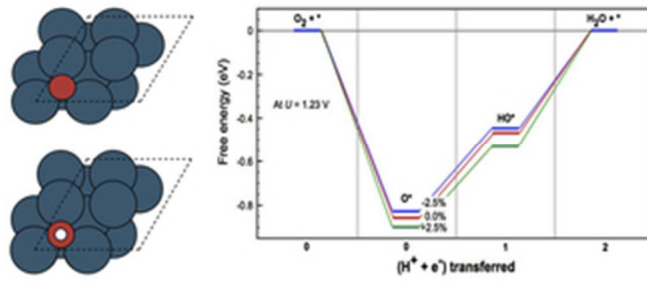
35x24mm (300 x 300 DPI)



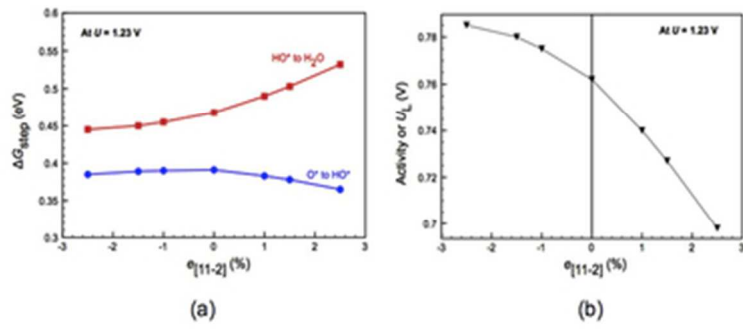
57x32mm (300 x 300 DPI)



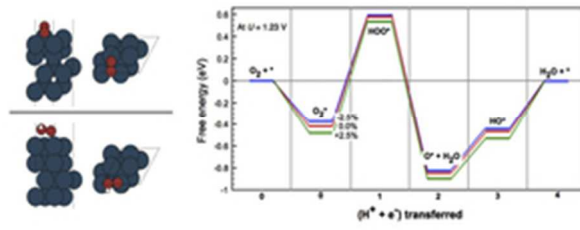
33x22mm (300 x 300 DPI)



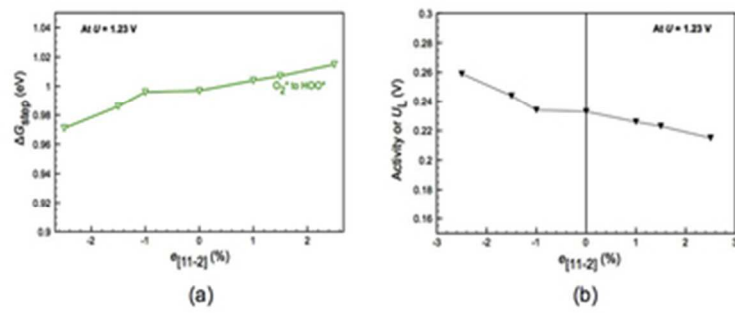
27x12mm (300 x 300 DPI)



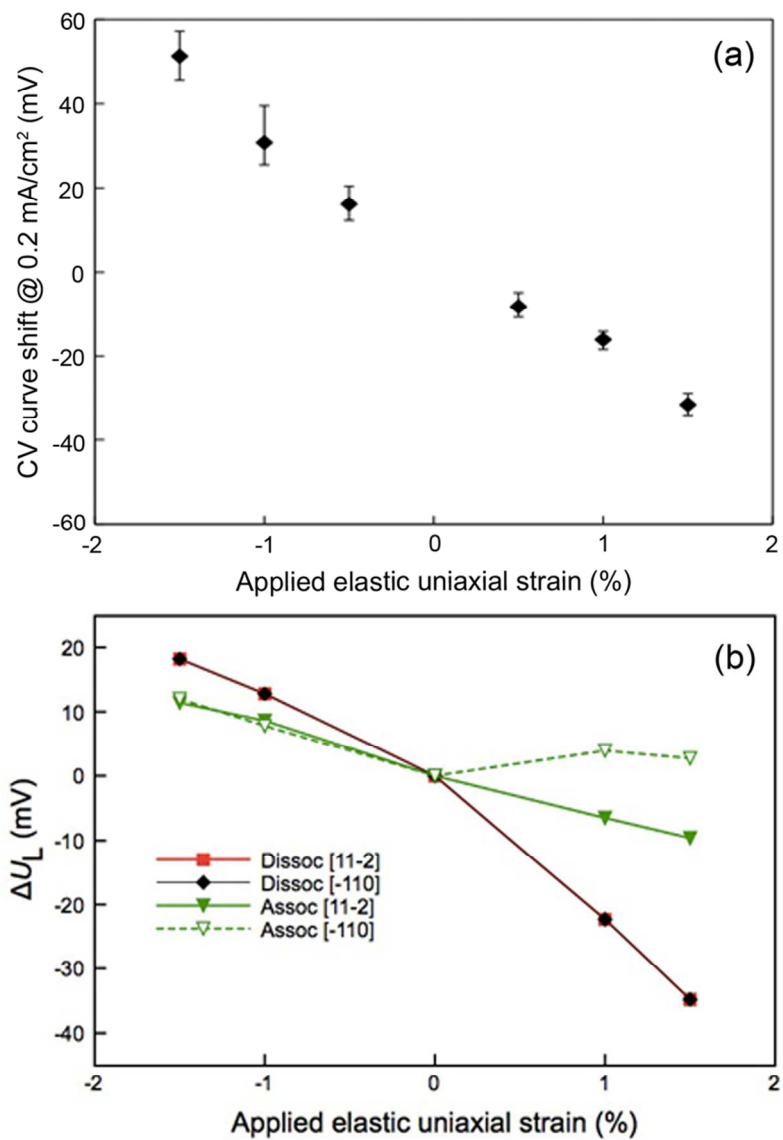
32x13mm (300 x 300 DPI)



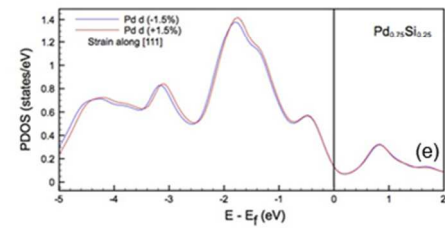
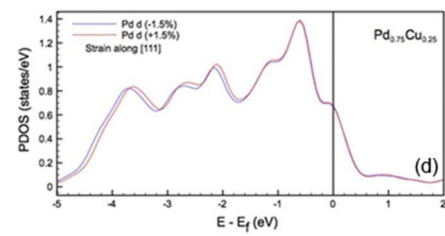
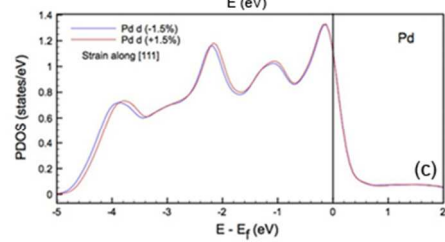
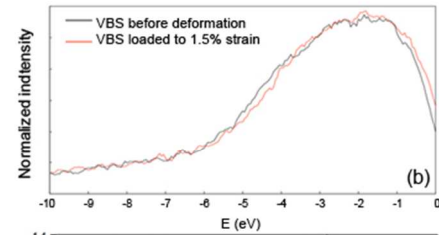
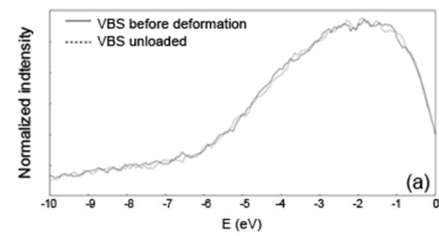
25x10mm (300 x 300 DPI)



31x13mm (300 x 300 DPI)



82x107mm (300 x 300 DPI)



63x164mm (150 x 150 DPI)